https://dx.doi.org/10.1016/j.trgeo.2020.100360

Investigation of the parallel gradation method based on the response of track-bed materials under cyclic loadings

Shuai Qi[1, 2], Yu-Jun Cui[2], Jean-Claude Dupla[2], Ren-Peng Chen[1], Han-Lin Wang[3], Yu Su[2], Francisco Lamas-Lopez[2], Jean Canou[2]

1: Zhejiang University, China

2: Laboratoire Navier/CERMES, Ecole des Ponts ParisTech (ENPC), France

3: Department of Civil and Environmental Engineering, The Hong Kong Polytechnic University, Hung Hom, Kowloon, Hong Kong, China

Corresponding author:

Mr. Shuai Qi
Department of Civil Engineering
Zhejiang University, Hangzhou, China

E-mail: qishuailw@163.com

Abstract

Ballast/fines mixture is often found in railway substructure and the overall behaviour of tracks is strongly dependent on the mechanical behaviour of this mixture. Since directly testing such mixture with large grains is limited with common laboratory equipment, the consideration of a model material at smaller size is advisable. Parallel gradation method is widely used for this purpose. This study assesses the validity of this method in the case of ballast/fines mixture. Large-scale cyclic triaxial tests were carried out on the ballast/fines mixture at six volumetric coarse grain contents. The results obtained were analysed, together with those obtained previously from small-scale triaxial tests on a microballast/fines mixture whose microballast grain size distribution was determined by applying the parallel gradation method. The cyclic parameters (permanent strain and resilient modulus) were obtained for the two types of mixture. Results show that for all mixtures two distinct soil fabrics can be identified according to the variations of permanent strain and resilient modulus with the volumetric content of coarse grains f_v: a fine-fine contact structure for $f_v \leq 20\%$ and a grain-grain contact structure for $f_v \geq 35\%$. In the case of fine-fine contact structure, the permanent strains and resilient modulus values of the ballast samples are consistent with those of the microballast samples, evidencing the validity of the parallel gradation method. In the case of grain-grain contact structure, the permanent strains and resilient modulus values are found to coincide globally at the two scales, also justifying the validity of the parallel gradation method in this case, the slight differences between the two scales being attributed to the irregular grain sliding and the distribution of the fines

45 soils.

46

47 **Keywords:** interlayer soil; cyclic triaxial tests; permanent deformation; resilient
48 modulus; parallel gradation method

1. Introduction

Ballast/fines mixture is often found in railway substructure [9,16]. For instance, in the French conventional railway lines (representing 94% of the total railway network), there is an interlayer which was formed by interpenetration of ballast and subgrade soils under the effect of train circulation [9]. During the renewable program for conventional lines, this layer was maintained since the dry density of the interlayer was as high as 2.4 Mg/m^3 and thus a favourable mechanical behaviour was expected [6]. According to the in-situ investigation, the soil fabric of the interlayer is found to be greatly dependent on the content of ballast grains [34,35]: the ballast grains are in contact with each other for the upper part with high ballast content, but floated in the fines matrix for the lower part with lower ballast content. Since the ballast/fines mixture plays an important role in the overall behaviour of rail tracks, it is important to investigate the mechanical response of such mixture under cyclic loading in terms of permanent deformation and resilient modulus. Considering the large size of ballast grains, large-scale triaxial apparatus is normally needed for this purpose. However, since the large testing system is complex and costly, scaling the ballast grains down to a model ballast material with smaller size and performing tests using standard apparatus appear quite promoting.

Three methods are commonly used for the scaling purpose: the scalping method [43] which consists in discarding the grains larger than a specified size from the prototype materials, the parallel gradation method [22] which consists in creating a model material at smaller size with its grain size distribution parallel to that of the prototype material, and the replacement method [13] which consists in replacing the

71 grains from a specified size to the maximum size with the grains from this specified
72 size to a smaller size. Among them, the parallel gradation method is regarded to be the
73 most appropriate because it can consider a large range of prototype gradation shape;
74 thus, it has been adopted mostly [1,15,27,36,37,38,39,40]. The validity of this method
75 under cyclic loadings was assessed by Sevi and Ge [32] based on the response of the
76 prototype and model grains of ballast grains. Their results in terms of resilient modulus,
77 permanent axial strain and permanent volumetric strain were unfortunately not
78 conclusive for validating the parallel gradation method. In addition, only pure ballast
79 grains were tested without fines fraction.

80 In this study, the parameters characterizing the cyclic response (permanent strain
81 and resilient modulus) of ballast/fines mixtures representing the interlayer soils in the
82 conventional French railway track-beds were determined by conducting large-scale
83 cyclic triaxial tests. Six volumetric ballast contents (0%, 5%, 10%, 20%, 35%, 45%)
84 were considered. The results obtained were analysed together with those obtained
85 previously by Wang et al. [37,38] from small-scale cyclic triaxial tests on
86 microballast/fines mixture with microballast prepared by applying the parallel
87 gradation method. Comparison of the mechanical parameters obtained at two scales
88 allowed the validity of the parallel gradation method to be assessed on ballast/fines
89 mixtures.

90

91 **2. Materials**

92 The ballast grains having the same grain size distribution as the interlayer soil in

93 "Sénissiat site" were used [34], as shown in Fig. 1. The minimum grain size $D^b_{\min}$ and
94 the maximum grain size $D^b_{\max}$ are 20 mm and 63 mm, respectively. The microballast
95 was tested previously by Wang et al. [37,38]; its maximum grain size $D^m_{\max}$ was chosen
96 as 20 mm to adapt to a small-scale triaxial cell of 100 mm with a value of 5 as the ratio
97 of sample to maximum grain size. This is consistent with the recommendation of
98 Fagnoul and Bonnechere [11], Nitchiporovitch [23] and Pedro [26]: a ratio larger than
99 5 must be adopted to minimize the sample size effect. The grain size distribution of the
100 microballast is transited from that of the ballast following the parallel gradation method.
101 In this method, the correlative grain sizes of ballast and microballast share the same
102 percentage of grain passing. The grain sizes of these two materials are correlated
103 according to the following equation:

104 (1) $$\frac{D^b - D^b_{\min}}{D^m - D^m_{\min}} = \frac{D^b_{\max} - D^b_{\min}}{D^m_{\max} - D^m_{\min}} = A$$

105 where $D_{\max}$, $D_{\min}$ and D are the maximum grain size, the minimum grain size, and a
106 given grain size, respectively. The superscripts b and m stand for ballast and
107 microballast, respectively. A is a constant.

108 To prepare the microballast, three commercial coarse grained soils were used,
109 with the minimum grain size $D^m_{\min}$ equal to 1.6 mm. This defines a value of 2.337 for
110 parameter A. For a given grain size of microballast D^m, 10.0 mm for instance, equation
111 (1) gives a correlated ballast grain size D^b of 39.6 mm. As the ballast grain passing
112 percentage is 59.1 % for D^b = 39.6 mm, according to the parallel gradation method,
113 the microballast grain passing percentage is also 59.1 % for D^m = 10 mm. Following
114 this procedure, the complete grain size distribution of the microballast was obtained, as

115 shown in Fig. 1. This target (parallel gradation) curve was verified by measurement and
116 it is observed that the measured grain size distribution and the target one show a good
117 agreement (Fig. 1).

118 For the fines soils, since obtaining enough quantity from the field was difficult,
119 they were fabricated in the laboratory by mixing nine commercial soils. Firstly, the mass
120 proportion of each constituting soil was calculated according to the grain-size
121 distributions of the fines from "Sénissiat site" (Fig. 2). With the proportion and the grain
122 size distribution of each soil, the grain size distribution of the fabricated fines can be
123 calculated, which was plotted in Fig. 2 as well. Then, these soils were poured into the
124 mixing machine in a certain sequence and mixed, during which water was carefully
125 added and in the end a small water content of 4% was reached (see more details in
126 Lamas-Lopez [20]). The aim of water addition was to prevent the small particles loss
127 during the mixing. Using this procedure, a homogeneous mixture can be obtained [20].
128 Wang et al. [37,38] also adopted this method when preparing samples of microballast
129 and fines mixture. The grain size distribution of the fabricated fines measured after the
130 preparation showed a good agreement with that of the in situ ones (see also Fig. 2). The
131 fabricated fine soil has a liquid limit w_L = 32.0% and a plasticity index I_p = 20.0%. This
132 soil is classified as lean clay (CL) according to ASTM D2487-11 [3]. Standard Proctor
133 compaction tests were carried out on the fines material following ASTM D698-12 [4].
134 An optimum water content $w_{\text{opt-f}}$ = 13.70% and a maximum dry density $\rho_{\text{dmax-f}}$ = 1.82
135 Mg/m^3 were determined.
136

3. Experimental methods

3.1. Sample preparation

In order to quantify the coarse grains in a sample, a parameter namely volumetric content of coarse grains f_v was adopted, which was defined as the ratio of the total volume of coarse grains to the total sample volume [26,27,30,37,38,39]. The total sample volume consisted of two parts: the coarse grain volume and the fines volume. All pores were assumed to be included in the fines soils. For the upper part of the natural interlayer soils at "Sénissiat site", the f_v value was 52.9% [34]. In this study, six f_v values (0%, 5%, 10%, 20%, 35%, 45%) were considered for the samples prepared with both ballast and microballast. For convenience, in further analysis, the samples prepared with ballast and microballast are referred to as ballast samples and microballast samples, respectively. The dimensions of the ballast samples are 300 mm diameter and 600 mm height, while the dimensions of microballast samples are 100 mm diameter and 200 mm height.

For the preparation of the ballast sample, the total volume was first calculated with the sample dimensions (300 mm diameter and 600 mm height). For a given f_v value, the volumes of both ballast grains and fines can be obtained based on this total sample volume. After that, the mass of ballast was obtained using the dry unit mass of ballast (2.68 Mg/m^3). The fines in all samples were kept at the same state defined by the optimum water content $w_{\text{opt-f}}$ = 13.70% and the maximum dry density $\rho_{\text{dmax-f}}$ = 1.82 Mg/m^3. The optimum state was selected aiming to simulate the heavily compact state in the field condition [7,20,35]. Accordingly, the masses of dry fines and water can be

159 determined. Water was firstly added into the fines by spray to reach the optimum water
160 content $w_{opt\text{-}f}$ = 13.7%. Then, the wetted fines soil was stored in hermetic containers for
161 24 h for moisture homogenization. Afterwards, the homogenized wetted fines soil was
162 equally divided into eight parts (by weight) and so were the oven-dried ballast grains,
163 after which they were mixed separately. Finally, these eight parts of mixed materials
164 were carefully compacted with a vibration hammer layer by layer.

165 Similar protocol was applied for the preparation of the microballast sample (100
166 mm diameter and 200 mm height). The masses of the dry microballast, dry fines soil
167 and water were first determined. Afterwards, the fines soil was wetted with the sprayed
168 water to reach the optimum water content of 13.7%, stored in hermetic container for 24
169 h and then mixed with the microballast. Finally, this mixture was compacted
170 dynamically to reach the target height. More details can be found in Wang et al. [37,38].
171

172 **3.2. Cyclic triaxial tests**

173 For the microballast sample with 100 mm diameter and 200 mm height, a small-scale
174 cyclic triaxial apparatus was used. Details about this device can be found in Wang et al.
175 [38]. For testing a ballast sample (300 mm diameter and 600 mm height), a large-scale
176 cyclic triaxial apparatus developed by Dupla et al. [10] was adopted. The loading
177 procedures adopted are the same for the ballast and the microballast samples. No
178 saturation process was applied and the sample water content was kept constant during
179 the test. In addition, the drainage valve was kept open during the loading process. All
180 the tests were performed at a confining pressure of 30 kPa, which corresponded to the

181 average horizontal stress estimated for the field condition, considering the effects of the
182 train wheel load, the interlayer depth and the Poisson ratio [8,37,38]. The applied cyclic
183 loads followed a sine-shaped pattern (Fig. 3). The deviator stress amplitude q is defined
184 as the difference value between the maximum deviator stress q_{max} and the minimum
185 deviator stress q_{min} (Wang et al. 2017, 2018a; Wang and Chen 2019; Wang et al. 2019).
186 A frequency of 1.78 Hz corresponding to a low train speed of 50 km/h was chosen,
187 aiming to guarantee the quality of controlling the pre-defined loading shape. Note that
188 this low frequency did not reflect the high train speed normally encountered in the field.
189 This selection was based on the hypothesis that the train speed does not influence the
190 assessment of the validity of the parallel gradation. During the loading procedure, axial
191 stress and strain were monitored.

192 The application of cyclic loads included two consecutive stages. The loading
193 stage 1 was focused on the aspect of the permanent deformation under a large number
194 of loading cycles. The loading stage 2 was focused on the aspect of the resilient modulus
195 or stiffness property under a wide range of stress amplitudes, including some large
196 amplitudes possibly applied on the interlayer soils. In stage 1, a multi-step loading
197 procedure proposed by Gidel et al. [12] was adopted (Fig. 4a): the deviator stress
198 amplitude $\Delta q = q_{max} - q_{min}$ was increased stepwise from 10 kPa to 30 kPa with an
199 increment of 5 kPa. At each amplitude, 90,000 cycles were applied, which were thought
200 to be enough for the stabilization of the permanent strain [9,12,20,35]. This multi-stage
201 loading procedure allowed the application of several stress amplitudes on the same
202 sample, with which not only the number of tests could be reduced, but also the effect

of the variability of soil samples on the testing results can be minimised. Thus, this procedure has been widely used in the study of the permanent deformation behaviour [5,9,18,20,33,35,38]. These loading amplitudes were selected based on the vertical stress measured at the equivalent depth of interlayer in the field [19,20]. In stage 2 (Fig. 4b), a procedure proposed by Lamas-Lopez [20] was adopted. The deviator stress amplitude Δq was firstly increased following a Δq sequence (10 kPa, 30 kPa and 50 kPa) and then decreased following the reverse sequence. Afterwards, Δq was increased following a sequence from 10 kPa to 100 kPa and then decreased to 10 kPa. Finally, Δq was increased in steps to 200 kPa and then decreased to 10 kPa. At each stress level, 100 cycles were applied. The aim of firstly increasing Δq and then decreasing it was to obtain the resilient modulus at both elastoplastic stage and pure elastic stage. Note that the large stress amplitudes (50 kPa, 100 kPa and 200 kPa) were defined according to the vertical stress of 40-90 kPa at similar depth of the interlayer observed by Selig and Waters [31], Jain and Keshav [17] and Yang et al. [42], the vertical stress of 120-138 kPa applied by heavier wagons in some countries [14,17,21] and the contingent maximum vertical stress at the top of railway structure as high as 200 kPa [20].

4. Results and discussions

4.1. Variations of permanent deformation with f_v

Fig. 5 plots the deviator stress q versus the axial strain ε_1 during the first 90,000 cycles of loading stage 1 for the ballast sample at f_v = 35%. In a loading-unloading cycle, the permanent axial strain ε_{1p} represented the irreversible part of the total axial strain. It

can be observed that the ε_{1p} value of the first cycle was particularly large. This phenomenon was also observed for other ballast samples and the microballast samples. This large permanent strain can be attributed to the adaptation of the sample to the loading system, in particular in terms of contact between the sample and the loading piston. As the initial sample-piston contact was not identical for all the samples, this ε_{1p} value would make impossible the relevant comparison of permanent strain between different samples. Thus, in further analysis, the first cycle was not accounted for the cumulative permanent strain.

Fig. 6 presents the permanent strain ε_{1p} against the number of cycles N for six ballast samples, with the corresponding stress levels. The evolutions of permanent strain with number of cycles N were the same as the ones of microballast samples [38]. It can be observed that, on the whole, a smaller f_v value led to a larger ε_{1p}. For each f_v value, ε_{1p} increased quickly at the beginning and then tended to stabilize with the increasing cycles.

Due to the multi-step loading procedure adopted, the ε_{1p} at each stress level was greatly influenced by the previous loadings (Fig. 6). If this loading history is eliminated (as if the sample has been subjected to only one loading level), the effect of the ballast contents can be better evaluated. For this purpose, a permanent strain estimation method proposed by Gidel et al. [12] and then used by Lamas-Lopez [20] and Wang et al. [38] was adopted. The application of this method is explained in Fig. 7 by considering two successive loading levels (Loading level M and Loading level $M + 1$). For the estimated permanent strain ε_{1p}^{M+1} of the Loading level $M + 1$ at the first 90,000 cycles, it is

247 determined as:

248 (2) $$\varepsilon_{1p}^{M+1} = \varepsilon_{1p}^{M} + \delta\varepsilon_{1p}^{M+1}$$

249 where ε_{1p}^{M} is the measured permanent strain of the Loading Level M; $\delta\varepsilon_{1p}^{M+1}$ is the
250 translated permanent strain determined by resetting both the initial strain value and the
251 first cycle of the measured permanent strain of the Loading level $M + 1$ to 0.

252 For estimating the permanent strain of the Loading level $M + 1$ after 90,000
253 cycles, a linear increasing trend between permanent strain and number of cycles is
254 considered, with its slope kept at the same value as the one determined at the last cycles
255 of Loading level $M + 1$. More details can be found in Wang et al. [38].

256 The estimated permanent strain curves for f_v = 0% of the ballast sample are
257 presented in Fig. 8, along with the measured results. It can be observed that at the last
258 cycle of each stress level, the estimated strain is larger than the measured one. For
259 example, for Δq = 20 kPa, the measured permanent strain at the last cycle N = 270,000
260 was 0.182%, while the corresponding estimated one was 0.226%. This phenomenon
261 can be attributed to the different loading histories: for the estimated strain, the sample
262 was assumed to undergo one higher stress level of 20 kPa. When it comes to the
263 measured strain, successive lower stress levels of 10kPa, 15 kPa and 20 kPa were
264 applied, leading to a smaller strain value.

265 Gidel et al. [12] examined this permanent strain estimation method through cyclic
266 triaxial tests, concluding that the permanent strain estimated for a single stress level
267 agreed well with the measured one for the loading cycles applied at each step (90,000
268 cycles in this study). In other words, in this study, the estimated permanent strain at the

first 90,000 cycles was relatively accurate. Fig. 9 depicts the estimated permanent strain evolutions at the first 90,000 cycles under different stress levels for ballast sample at f_v = 0%. As can be observed, a larger stress level led to a larger strain value. In addition, the permanent strain gradually stabilized with the increase of the cycle number. To further illustrate the effect of ballast content f_v, the estimated permanent strains for cycle N = 90,000 (end-stage cycle in Fig. 9) at all stress levels were taken and compared (Fig. 10). It can be observed that at each stress level, the permanent strain decreases with the increase of f_v. Moreover, a bi-linear decreasing trend can be identified. When $f_v \leq 20\%$, the permanent strain decreases rapidly. By contrast, when $f_v \geq 35\%$, this decreasing rate becomes smaller. The same observations were made by Wang et al. [38] for the microballast samples.

In the study of Wang et al. [38], X-ray microcomputed tomography (μCT) scans were carried out on the as-compacted microballast samples. Two soil fabrics were identified at different f_v values: a fine-fine contact structure at f_v = 0%-20% and a distinct grain-grain contact structure at f_v = 35%-45%. It is worth noting that at f_v = 20%, the coarse grains started to be partially connected without forming a whole skeleton. Unfortunately, this μCT scan could not be conducted on ballast samples due to their large size. However, basically, it seems plausible to consider the same feature of fabrics for the ballast samples: also a fine-fine contact structure at low f_v and a grain-grain contact structure at high f_v. For fine-fine contact structure, the permanent strain results from the compression of the fines, which decreases rapidly with increasing f_v. By contrast, for grain-grain contact structure, the rearrangement of the grains plays a

dominant role and the permanent strain decreases slightly when f_v increases.

4.2. Variations of resilient modulus with f_v

Typical hysteresis loops at the first cycles of different stress levels are shown in Fig. 11 for the ballast sample at f_v = 20%. The loops for stress levels of Δq = 10 kPa, Δq = 30 kPa, Δq = 50 kPa, Δq = 100 kPa and Δq = 200 kPa corresponded to cycle numbers of N = 1, N = 101, N = 201, N = 701 and N = 1401, respectively. It appeares that for the low stress levels of 10 kPa and 30 kPa, the hysteresis loops were pretty small and closed. This was due to the application of 450,000 loading cycles under $\Delta q \leq 30$ kPa in loading stage 1. By contrast, for stress levels larger than 30 kPa, permanent strain developed, leading to larger and unclosed hysteresis loops, in particular under stress levels as high as Δq = 100 kPa and 200 kPa.

The evolution of hysteresis loop with number of cycles is illustrated in Fig. 12 by plotting the loops for 100 cycles (from N = 701 to N = 800) at Δq = 100 kPa for the ballast sample with f_v = 20%. A large and unclosed hysteresis loop was observed for the first cycle, due to the stress level of 100 kPa which was larger than all the previous applied stress levels. In addition, with the increase of the cycle number, the hysteresis loop became smaller and smaller and at the end of loading, the loops became closed and relatively unchanged, suggesting a pure elastic behaviour of soil.

As shown in Fig. 13, the resilient modulus M_r is defined as [28,29]:

$$M_r = \Delta q / \varepsilon_{1r} \quad (3)$$

where Δq is the deviator stress amplitude, and ε_{1r} is the resilient strain.

313 The evolution of M_r with the number of cycles N at varying stress levels is
314 presented in Fig. 14 for the ballast sample at f_v = 20%. The results of other ballast
315 samples and microballast samples obey the same rule and are not shown for clarity. It
316 can be observed that when the stress amplitude increased, the M_r value immediately
317 decreased and then tended to stabilize. By contrast, with the stress amplitude decreasing,
318 the M_r value increased instantly and then tended to reach a stabilization state. The
319 decrease of M_r with the increase of stress amplitude can be explained by the strain
320 increasing due to the increase of stress amplitude [2].
321 In order to illustrate the effect of f_v on resilient modulus, the M_r values of the last
322 (end-stage) cycles of all stress levels were taken and presented as a function of f_v for
323 different stress levels (Fig. 15). The data were named according to the number of cycles
324 N and the corresponding Δq values. It appears that an increasing trend of M_r with f_v can
325 be identified for all stress levels. Moreover, this increasing trend followed a bi-linear
326 pattern with the slope at $f_v \geq 35\%$ larger than the one at $f_v \leq 20\%$, evidencing that the
327 soil fabrics of the ballast samples at these two f_v ranges were different: fine-fine contact
328 structure at low f_v and grain-grain contact structure at higher f_v. Same bi-linear variation
329 trend of M_r was identified by Wang et al. [37] for the microballast samples, similarly,
330 evidencing that the soil fabrics of microballast samples at $f_v \leq 20\%$ and $f_v \geq 35\%$ were
331 separately dominated by fine-fine contact structure and grain-grain contact structure.
332
333 **4.3. Comparison of permanent strain between ballast and microballast samples**
334 The estimated permanent strains for cycle N = 90,000 (end-stage cycle) at six f_v values

335 are presented in Fig. 16 for the ballast and the microballast samples, for five stress
336 levels (10, 15, 20, 25 and 30 kPa). It can be observed that in the case of f_v = 0%, at each
337 stress level, the ε_{1p} value of the ballast sample coincides well with that of the
338 microballast sample. For the fine-fine contact structure at f_v = 5% and 10%, on the
339 whole, the ε_{1p} values of the corresponding different scale samples are found to be similar.
340 This phenomenon can be explained by the fact that in this case the fines matrix
341 constitutes the soil skeleton and the permanent strain is dominated by the compression
342 of the fines, giving rise to the permanent strains which are independent of coarse grain
343 size. For the grain-grain contact structure at f_v = 35% and 45%, it can be observed that
344 the permanent strains of the ballast samples and the microballast samples are almost
345 the same (Fig. 16), in particular at Δq = 10 kPa (Fig. 16a). Note that although the case
346 at f_v = 20% is categorized into the group of fine-fine contact structure, the influence of
347 coarse grain size on the permanent strain follows the same pattern. This can be
348 explained by the fact that at f_v = 20%, part of the coarse grains starts to be in contact
349 with each other. Further examination shows that at Δq higher than 10 kPa, the strains
350 of microballast samples are slightly larger than those of the ballast samples. This
351 phenomenon can be explained as follows: upon loadings, the grains would slide into
352 the pores nearby, giving rise to permanent strain. If the difficulty of sliding into large
353 pores for the large grains is the same as that for the smaller grains to slide into smaller
354 pores, identical permanent strains can be expected. It is the case for the ballast sample
355 and the microballast sample at Δq = 10 kPa. Apparently, the grains sliding depends on
356 the stress level and the grain sizes; in the microballast sample, the grains with smaller

sizes would slide into the adjacent pores more easily, leading to a slightly larger strain.

Another possible explanation for the slightly larger strains in the microballast sample is related to the effect of the fines soils. As shown in Fig. 17, the fines soils can be roughly considered to be distributed at two locations: the pores near the coarse grain and the coarse grain intervals along the stress chain (supposed to be along the sample height). The applied load was transmitted along the stress chain by compressing the fines between grains. When the load reached a certain level, grain rearrangement occurred [24,25]. It can be inferred that the fines in the pores inhibited the coarse grain sliding, while those between grains promoted it. At a given f_v value, for the microballast sample, more grain-fines-grain contacts can be expected along the stress chain, leading to more distribution of fines soils. As a result, relatively larger permanent strain can be expected.

As the difference of permanent strain between the two scale samples appears quite small (Figure. 16), it can be reasonably concluded that the parallel gradation method is valid for the ballast/fines mixture in terms of permanent strain.

4.4. Comparison of resilient modulus between ballast and microballast samples

The comparison of M_r values between the microballast and ballast samples with fine-fine contact structure is shown in Fig. 18. At $f_v = 0\%$, the M_r values of the ballast sample are comparable with those of the microballast sample. This is normal because the scaling question are not involved in that case. For higher f_v values, except $f_v = 10\%$, the M_r values of the ballast and the microballast samples coincide with each other. The

379 singular case at f_v = 10% is probably due to a technical problem.

380 The M_r values of the ballast samples at grain-grain contact structure are compared
381 with those of the mciroballast samples in Fig. 19 (Fig. 19a for f_v = 35% and Fig. 19b
382 for f_v = 45%). It can be observed that almost the same M_r values are obtained for the
383 two samples, indicating that the resilient modulus is independent of grain size. Further
384 investigation shows that on the whole the M_r values of the microballast samples are
385 slightly smaller than those of the ballast samples. These phenomena can be explained
386 based on the analysis of Yang and Gu [41]. They derived the resilient modulus of a
387 simple cubic array of identical spheres under a certain confining pressure by applying
388 a small shear stress onto it. In the analysis, the induced resilient shear strain of the cubic
389 array was determined by adding up the tangential strains between every two spheres
390 along the vertical stress chain. This tangential strain was calculated using the Hertz-
391 Mindlin contact law, which was a function of the applied shear stress. The expression
392 for the resilient modulus (defined as the ratio of the shear stress to the shear strain) was
393 obtained, showing no dependence on sphere radius. Note that this analysis did not
394 consider any contribution from fine soils, thus not fully reflecting the case of this study.
395 Indeed, as mentioned previously, in the case of mixture, the resilient modulus is affected
396 by the fine soils along the stress chain. For the microballast samples, as stated before,
397 there are more fines soils along it. Thus, relatively smaller resilient modulus values are
398 expected.

399 As for the permanent strain, globally, the resilient modulus also showed a good
400 agreement between the two scale samples albeit the slight difference discussed above,

401 which validates the parallel gradation method in terms of resilient modulus.

402

403 **5. Conclusions**

404 Large-scale cyclic triaxial tests were carried out on a ballast/fines mixture (ballast
405 sample), while small-scale cyclic triaxial tests were conducted on a microballast/fines
406 mixture with microballast prepared following the parallel gradation method
407 (microballast sample). Six volumetric coarse grain contents were considered for each
408 kind of samples. The applied cyclic loadings included two stages, with stage 1 focusing
409 on the permanent strain under a large number of loading cycles and stage 2 focusing on
410 the resilient modulus under a wide range of stress amplitudes. The comparisons of the
411 mechanical parameters for the two different scale samples allowed the parallel
412 gradation method to be assessed.

413 Two soil fabrics could be defined as fine-fine contact structure at f_v = 0-20% and
414 grain-grain contact structure at f_v = 35-45%. It was observed that for the ballast and
415 microballast samples, with the increase of f_v value, for permanent strain it decreased
416 rapidly when $f_v \leq 20\%$ and this decreasing rate slowed down when $f_v \geq 35\%$, while for
417 resilient modulus it increased slightly when $f_v \leq 20\%$ and increased significantly when
418 $f_v \geq 35\%$.

419 The consistency between the large-scale and small-scale triaxial tests were found
420 to be satisfactory: at f_v = 0%, the permanent strains as well as resilient modulus values
421 obtained from the two apparatuses showed a good correspondence. In the case of fine-
422 fine contact structure, the parallel gradation method was found to be valid. The

permanent strains and resilient modulus values of the ballast samples were consistent with the respective ones of the microballast samples. This could be explained by the fact that in this case the fines matrix constituted the soil skeleton.

In the case of grain-grain contact structure, on the whole, the permanent strains of the ballast samples coincided with those of the microballast samples (especially at Δq = 10 kPa). This coincidence was also observed in terms of resilient modulus. For the permanent strain, it could be explained by the fact that the difficulties of the sliding of large ballast grains into the adjacent large pores and the sliding of the small microballast grains into the smaller pores were expected to be the same. For the resilient modulus, it could be explained by the analytical results of Yang and Gu (2013), showing that the resilient modulus is independent of grain size. Further examination of the permanent strain results showed that the permanent strains under higher stress levels (Δq > 10 kPa) were slightly larger for microballast samples, which could be explained by the fact that in microballast samples, the sliding of smaller grains into adjacent pores was easier. Another possible explanation was that there were more fines soils along the stress chain, favouring the coarse grain sliding and thus giving rise to larger strains. Deeper examination of the resilient modulus results showed a slightly smaller value for the microballast sample. This could also be attributed to more fines soils distributed along the stress chain.

Acknowledgements

The support from the Chinese Scholar Council (CSC) is greatly acknowledged.

445

446 **Notations**

A	constant in the similitude equation from ballast to microballast
D^b	given grain size of ballast
$D^b_{\max}$	maximum grain size of ballast
$D^b_{\min}$	minimum grain size of ballast
D^m	given grain size of microballast
$D^m_{\max}$	maximum grain size of microballast
$D^m_{\min}$	minimum grain size of microballast
f_v	volumetric content of coarse grains
I_p	plasticity index
M_r	resilient modulus
N	number of cycles
q	deviator stress
q_{max}	maximum deviator stress
q_{min}	minimum deviator stress
w_L	liquid limit
$w_{\text{opt-f}}$	optimum water content of fines
Δq	deviator stress amplitude
$\delta\varepsilon_{1p}^{M+1}$	translated permanent strain from the measured curve of Loading level M+1
ε_1	axial strain

ε_{1p}	permanent axial strain
ε_{1r}	resilient strain
ε_{1p}^{M}	measured permanent strain of the Loading Level *M*
ε_{1p}^{M+1}	estimated permanent strain of Loading level M+1
$\rho_{\text{dmax-f}}$	maximum dry density of fines

References

[1] Aingaran, S. 2014. Experimental investigation of static and cyclic behavior of scaled railway ballast and the effect of stress reversal. Ph.D. thesis, University of Southampton.

[2] Atkinson, J.H. 2000. Non-linear soil stiffness in routine design. Géotechnique, 50(5): 487-507.

[3] ASTM. 2011. D2487-11: Standard practice for classification of soils for engineering purposes (unified soil classification system). ASTM International, West Conshohocken, PA, USA.

[4] ASTM. 2012. D698-12: Standard test methods for laboratory compaction characteristics of soil using standard effort. ASTM International, West Conshohocken, PA, USA.

[5] Cao, Z.G., Chen, J.Y., Cai, Y.Q., Zhao, L., Gu, C., and Wang, J. 2018. Long-term behavior of clay-fouled unbound granular materials subjected to cyclic loadings with different frequencies. Engineering Geology, 243: 118-127.

[6] Cui, Y.J., Duong, T.V., Tang, A.M., Dupla, J.C., Calon, N., and Robinet, A. 2013.

464 Investigation of the hydro-mechanical behavior of fouled ballast. Journal of
465 Zhejiang University-Science A (Applied Physics & Engineering), 14(4): 244-255.
466 [7] Duong, T.V. 2013. Investigation of the hydro-mechanical behavior of ancient
467 railway platforms in scope to reinforcement by soil-mixing. Ph.D. thesis, Ecole
468 Nationale des Ponts et Chaussées, Université Paris-Est.
469 [8] Duong, T.V., Cui, Y.J., Tang, A.M., Dupla, J.C., Canou, J., Calon, N., and Robinet,
470 A. 2016. Effects of water and fines contents on the resilient modulus of the
471 interlayer soil of railway substructure. Acta Geotechnica, 11(1): 51-59.
472 [9] Duong, T.V., Tang, A.M., Cui, Y.J., Trinh, V.N., Dupla, J.C., Calon, N., Canou, J.,
473 and Robinet, A. 2013. Effects of fines and water contents on the mechanical
474 behavior of interlayer soil in ancient railway sub-structure. Soils and Foundations,
475 53(6): 868-878.
476 [10] Dupla, J.C., Pedro, L.S., Canou, J., and Dormieux, L. 2007. Mechanical behavior
477 of coarse grained soils reference. Bulletin de Liaison des Laboratoires des Ponts et
478 Chaussées, 268-269: 31-58.
479 [11] Fagnoul, A., and Bonnechere, F. 1969. Shear strength of porphiry materials. *In*
480 Proceedings of the 7th International Conference on Soil Mechanics and Foundation
481 Engineering, Mexico, pp. 61-65.
482 [12] Gidel, G., Hornych, P., Chauvin, J.J., Breysse, D., and Denis, A. 2001. A new
483 approach for investigating the permanent deformation behavior of unbound
484 granular material using the repeated load triaxial apparatus. Bulletin des
485 Laboratoires des Ponts et Chaussées, 233: 5-21.

[13] Frost, R.J. 1973. Some testing experiences and characteristics of boulder-gravel fills in earth dams. *In* Evaluation of relative density and its role in geotechnical projects involving cohesionless soils. STP 523. ASTM Standards and Publications.

[14] Grabe, P., and Clayton, C. 2009. Effects of principal stress rotation on permanent deformation in rail track foundations. Journal of Geotechnical and Geoenvironmental Engineering, 135(4): 555–565.

[15] Indraratna, B., Wijewardena, L.S.S., and Balasubramaniam, A.S. 1993. Large-scale triaxial testing of greywacke rockfill. Géotechnique, 43: 37-51.

[16] Indraratna, B., Su, L., and Rujikiatkamjorn, C. 2011. A new parameter for classification and evaluation of railway ballast fouling. Canadian Geotechnical Journal, 48(2): 322-326.

[17] Jain, V., and Keshav, K. 1999. Stress distribution in railway formation - a simulated study. *In* Proceeding of the 2nd International Symposium on Pre-Failure Deformation Characteristics of Geomaterials-IS Torino.

[18] Jing, P., Nowamooz, H., and Chazallon, C. 2016. Permanent deformation behaviour of a granular material used in low-traffic pavements. Road Materials and Pavement Design, 19(2): 289-314.

[19] Lamas-Lopez, F., Costa D'Aguiar, S., Robinet, A., Cui, Y.J., Calon, N., Canou, J., Dupla, J.C., and Tang, A.M. 2015. In-situ investigation of the behaviour of a French conventional railway platform. *In* Proceedings of Transportation Research Board TRB 2015, Washington, DC.

[20] Lamas-Lopez, F. 2016. Field and laboratory investigation on the dynamic

508 behaviour of conventional railway track-bed materials in the context of traffic
509 upgrade. Ph.D. thesis, Ecole Nationale des Ponts et Chaussées, Université Paris-
510 Est.
511 [21] Li, D., and Selig, E. 1998. Method for railroad track foundation design. I:
512 Development. Journal of Geotechnical and Geoenvironmental Engineering, 124(4):
513 316–322.
514 [22] Lowe, J. 1964. Shear strength of coarse embankment dam materials. *In*
515 Proceedings of the 8th International Congress on Large Dams 3, Edinburgh, U.K.,
516 pp. 745-761.
517 [23] Nitchiporovitch, A.A. 1969. Shearing strength of coarse shell materials. *In*
518 Proceedings of the 7th International Conference on Soil Mechanics and Foundation
519 Engineering, Mexico, pp. 211-216.
520 [24] Oda, M., Konishi, J., and Nasser, N.S. 1982. Experimental micromechanical
521 evaluation of strength of granular materials: effects of particle rolling. Mehcanics
522 of Materials, 1(4): 269-283.
523 [25] Oda, M., and Kazama, H. 1998. Microstructure of shear band and its relation to
524 the mechanisms of dilatancy and failure of dense granular soils. Géotechnique,
525 48(4): 465-481.
526 [26] Pedro, L. 2004. De l'étude du comportement mécanique de sols hétérogènes
527 modèles à son application au cas des sols naturels. Ph.D. thesis, Ecole Nationale
528 des Ponts et Chaussées, Université Paris-Est.
529 [27] Qi, S., Cui, Y.J., Chen, R.P., Wang, H.L., Lamas-Lopez, F., Aimedieu, P., Dupla,

530 J.C., Canou, J., and Saussine, G. 2019. Influence of grain size distribution of
531 inclusions on the mechanical behaviors of track-bed materials. Géotechnique in
532 press. doi : 10.1680/jgeot.18.P.047.
533 [28] Rollins, K.M., Evans, M.D., Diehl, N.B., and Daily III, W.D. 1998. Shear modulus
534 and damping relationships for gravels. Journal of Geotechnical and
535 Geoenvironmental Engineering, 124(5): 396-405.
536 [29] Seed, H.B., Wong, R.T., Idriss, I.M., and Tokimatsu, K. 1986. Moduli and damping
537 factors for dynamic analyses of cohesionless soils. Journal of Geotechnical
538 Engineering, 112(11): 1016-1032.
539 [30] Seif El Dine, B., Dupla, J.C., Frank, R., Canou, J., and Kazan, Y. 2010. Mechanical
540 characterization of matrix coarse-grained soils with a large-sized triaxial device.
541 Canadian Geotechnical Journal, 47: 425-438.
542 [31] Selig, E., and Waters, J. 1994. Track geotechnology and sub-structure management.
543 Thomas Telford, London, U.K.
544 [32] Sevi, A., and Ge, L. 2012. Cyclic behaviors of railroad ballast within the parallel
545 gradation scaling framework. Journal of Materials in Civil Engineering, 24(7):
546 797-804.
547 [33] Tang, L., Yan, M.H., Ling, X.Z., and Tian, S. 2017. Dynamic behaviours of
548 railway's base course materials subjected to long-term low-level cyclic loading:
549 experimental study and empirical model. Géotechnique, 67(6): 537-545.
550 [34] Trinh, V.N. 2011. Comportement hydromécanique des matériaux constitutifs de
551 plateformes ferroviaires anciennes. Ph.D. thesis, Ecole Nationale des Ponts et

552 Chaussées, Université Paris-Est.
553 [35] Trinh, V.N., Tang, A.M., Cui, Y.J., Dupla, J.C., Canou, J., Calon, N., Lambert, L.,
554 Robinet, A., and Schoen, O. 2012. Mechanical characterisation of the fouled ballast
555 in ancient railway track sub-structure by large-scale triaxial tests. Soils and
556 Foundations, 52(3): 511-523.
557 [36] Varadarajan, A., Sharma, K.G., Venkatachalam, K., and Gupta, A.K. 2003. Testing
558 and modeling two rockfill materials. Journal of Geotechnical and
559 Geoenvironmental Engineering, 129(3): 206-218.
560 Wang, H.L., Chen, R.P. 2019 Estimating static and dynamic stresses in geosynthetic-
561 reinforced pile-supported track-bed under train moving loads. Journal of
562 Geotechnical and Geoenvironmental Engineering, 145 (7) 04019029.
563 Wang, H.L., Chen, R.P., Cheng, W., Qi, S., Cui, Y.J., 2019. Full-scale model study on
564 variations of soil stress in geosynthetic-reinforced pile-supported track-bed with
565 water level change and cyclic loading. Canadian Geotechnical Journal. 56 (1), 60–
566 68.
567 [37] Wang, H.L., Cui, Y.J., Lamas-Lopez, F., Dupla, J.C., Canou, J., Calon, N., Saussine,
568 G., Aimedieu, P., and Chen, R.P. 2017. Effects of inclusion contents on resilient
569 modulus and damping ratio of unsaturated track-bed materials. Canadian
570 Geotechnical Journal, 54: 1672-1681.
571 [38] Wang, H.L., Cui, Y.J., Lamas-Lopez, F., Dupla, J.C., Canou, J., Calon, N., Saussine,
572 G., Aimedieu, P., and Chen, R.P. 2018a. Permanent deformation of track-bed
573 materials at various inclusion contents under large number of loading cycles.

574 Journal of Geotechnical and Geoenvironmental Engineering, 144(8): 04018044.
575 [39] Wang, H.L., Cui, Y.J., Lamas-Lopez, F., Calon, N., Saussine, G., Dupla, J.C.,
576 Canou, J., Aimedieu, P., and Chen, R.P. 2018b. Investigation on the mechanical
577 behavior of track-bed materials at various contents of coarse grains. Construction
578 and Building Materials journal, 164: 228-237.
579 [40] Xiao, Y., Liu, H.L., Chen, Y.M., and Jiang, J.S. 2014. Bounding surface model for
580 rockfill materials dependent on density and pressure under triaxial stress conditions.
581 Journal of Engineering Mechanics, 140: 04014002.
582 [41] Yang, J., and Gu, X.Q. 2013. Shear stiffness of granular material at small strains:
583 does it depend on grain size?. Géotechnique, 63(2): 165-179.
584 [42] Yang, L., Powrie, W., and Priest, J. 2009. Dynamic stress analysis of a ballasted
585 railway track bed during train passage. Journal of Geotechnical and
586 Geoenvironmental Engineering, 135(5): 680–689.
587 [43] Zeller, J., and Wullimann, R. 1957. The shear strength of the shell materials for the
588 Göschenenalp Dam, Switzerland. *In* Proceedings of the 4th International
589 Conference on Soil Mechanics and Foundation Engineering, London, pp. 399-404.

List of Figures

Fig. 13. Determination of M_r

Fig. 14. Evolution of M_r with number of cycles at different stress levels for ballast sample at f_v = 20%

Fig. 15. Evolutions of M_r at end stage with f_v for ballast samples at: (a) Δq = 10 kPa; (b) Δq = 30 kPa; (c) Δq = 50 kPa; (d) Δq = 100 kPa and 200 kPa

Fig. 16. Variations of estimated end-stage permanent strains with f_v for ballast and microballast samples at: (a) Δq = 10 kPa; (b) Δq = 15 kPa; (c) Δq = 20 kPa; (d) Δq = 25 kPa and 30 kPa

Fig. 17. Schematic illustration of the distribution of fines soils in case of grain-grain contact structure

Fig. 18. Comparison of M_r value between ballast samples and microballast samples in case of fine-fine contact structure for: (a) f_v = 0%; (b) f_v = 5%; (c) f_v = 10%; (d) f_v = 20%

Fig. 19. Comparison of M_r value between ballast samples and microballast samples in case of grain-grain contact structure for (a) f_v = 35% and (b) f_v = 45%

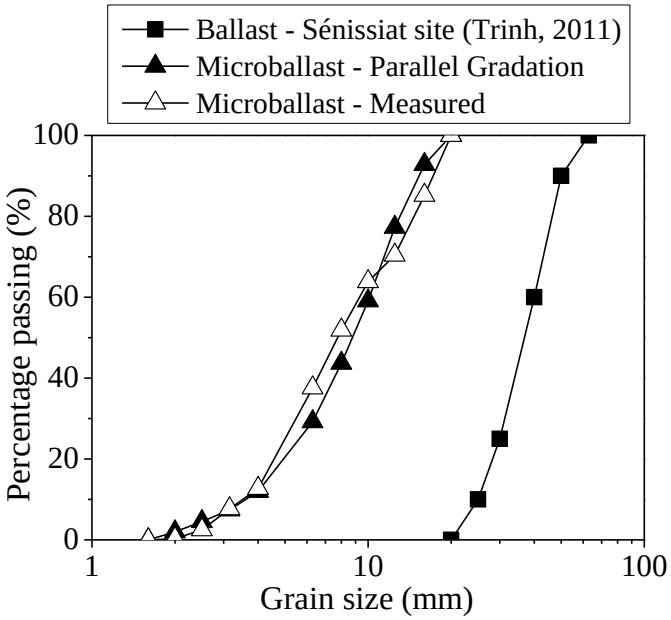

Fig. 1. Grain size distributions of the ballast and the microballast (modified from Wang et al. 2018a)

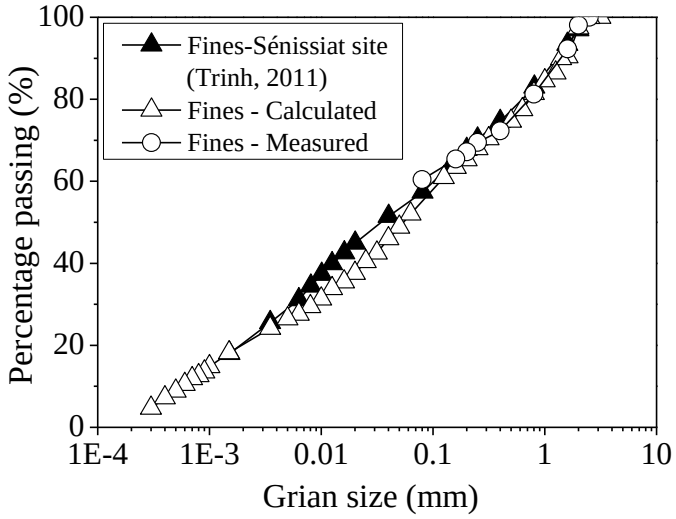

Fig. 2. Grain size distributions of fines (modified from Wang et al. 2018a)

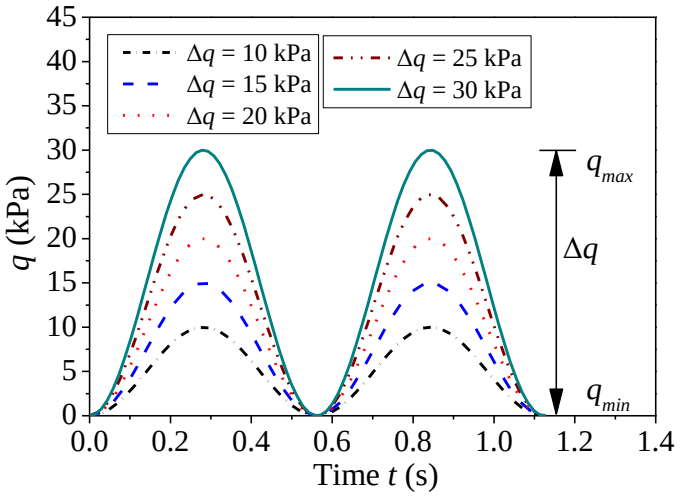

Fig. 3. Typical sine-shaped signals applied in the cyclic loadings

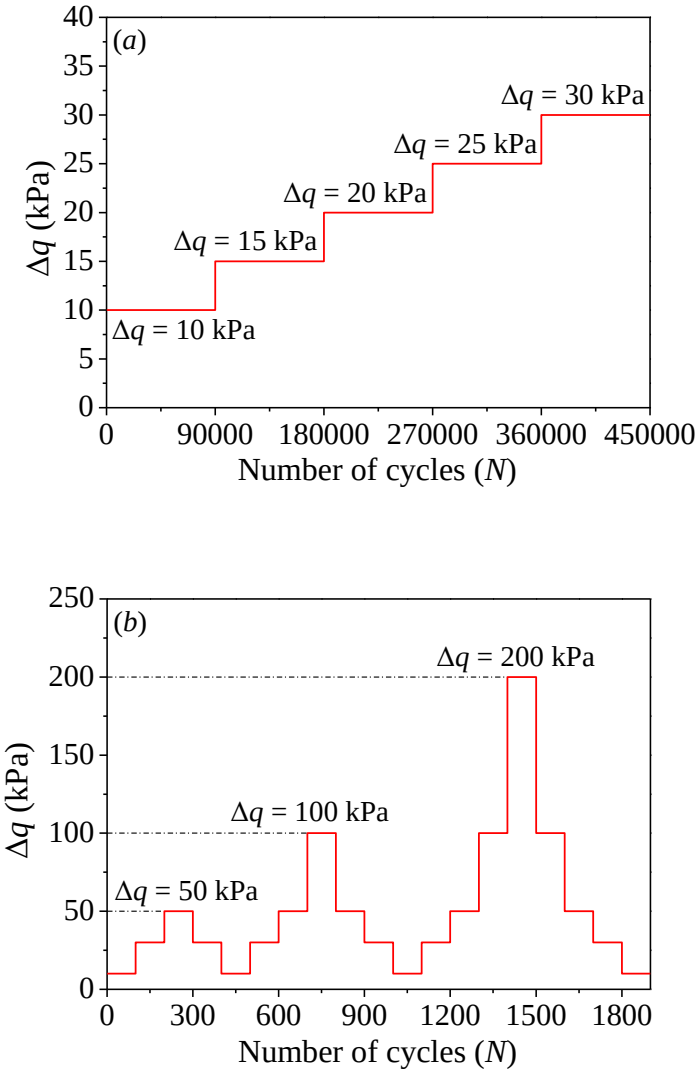

Fig. 4. Loading paths in two stages: (a) stage 1 for permanent strain investigation; (b) stage 2 for resilient modulus investigation

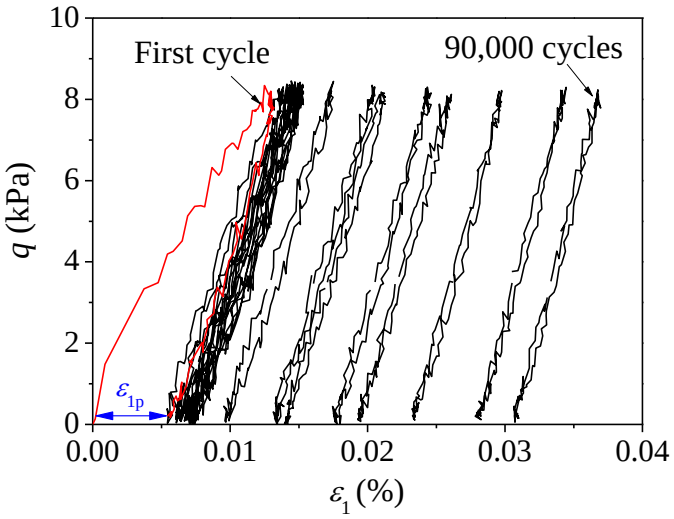

Fig. 5. Deviator stress q versus axial strain ε_1 for the first 90,000 cycles of loading stage 1 (ballast sample at f_v = 35%)

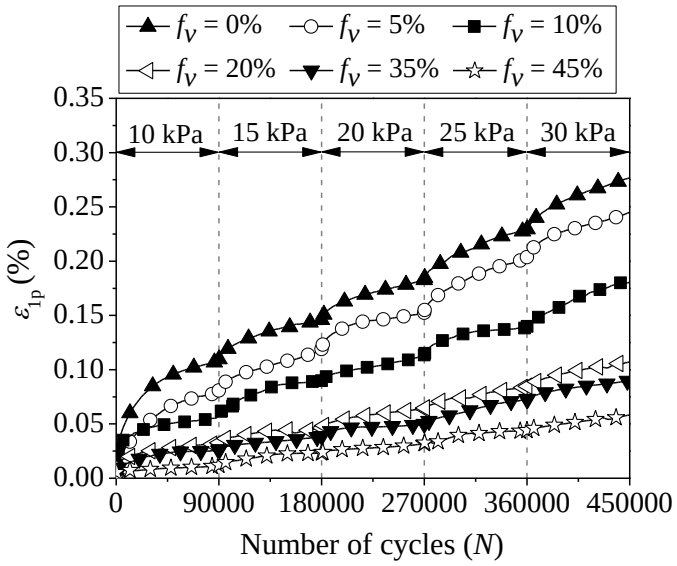

Fig. 6. Permanent strain evolutions with number of cycles at different f_v values

(ballast samples)

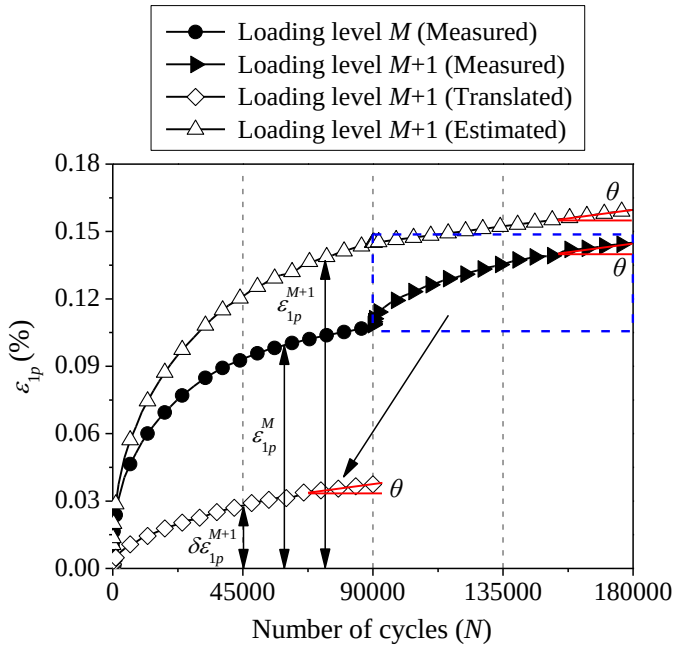

Fig. 7. Illustration of the method to eliminate the loading history effect

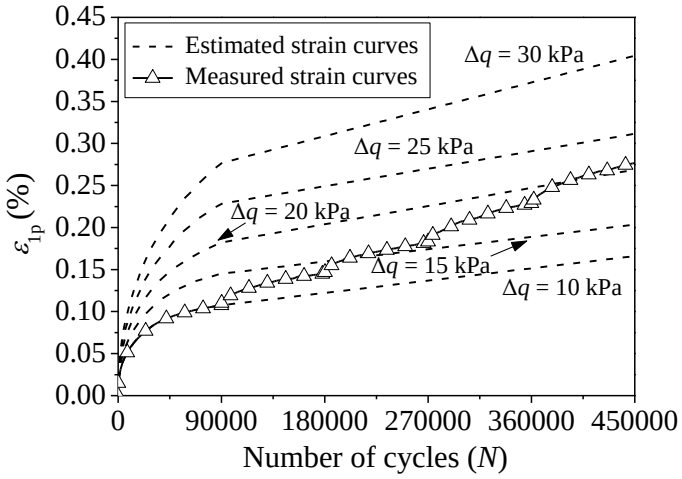

Fig. 8. Measured and estimated permanent strain curves for ballast sample at f_v = 0%

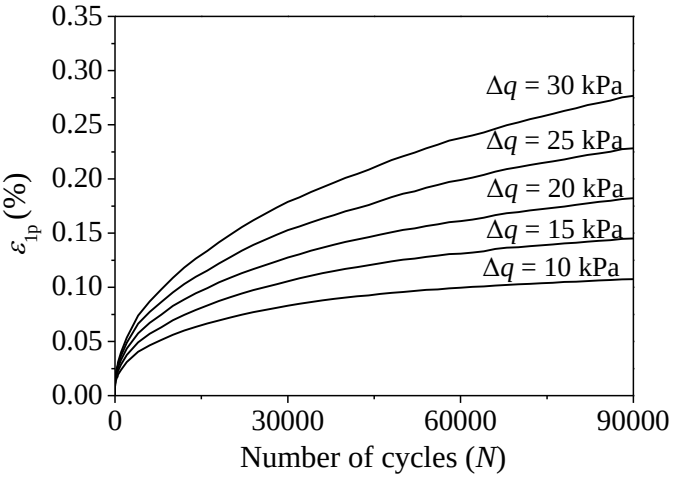

Fig. 9. Estimated permanent strain evolutions at the first 90,000 cycles for ballast sample at f_v = 0%

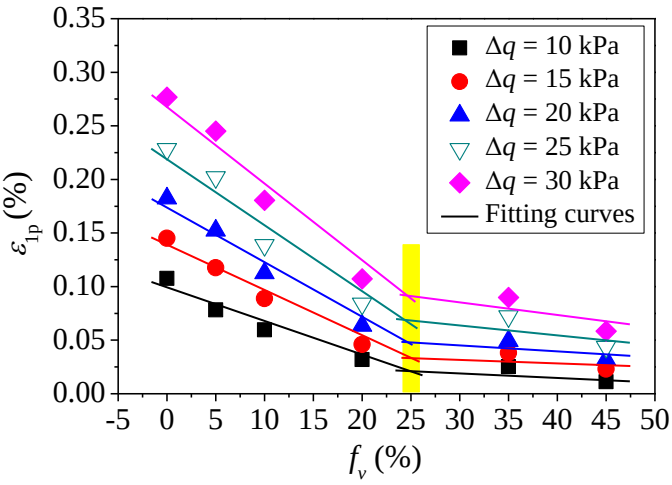

Fig. 10. Variations of estimated end-stage permanent strains with f_v at different stress levels (ballast samples)

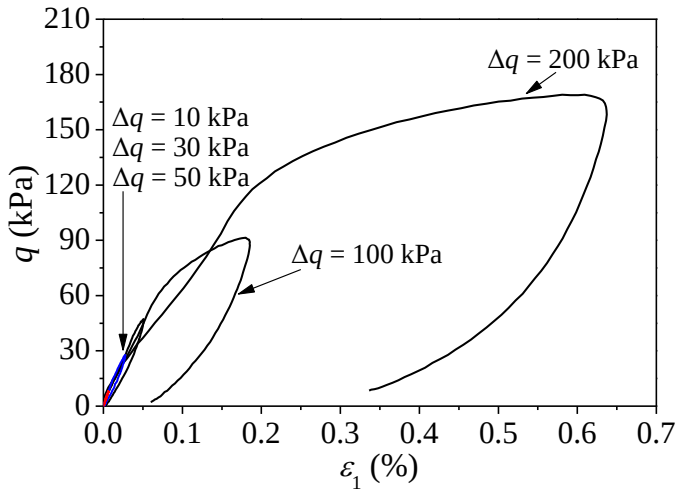

Fig. 11. Hysteresis loops at the first cycles of different stress levels for ballast sample at f_v = 20%: Δq = 10 kPa (N = 1), Δq = 30 kPa (N = 101), Δq = 50 kPa (N = 201), Δq = 100 kPa (N = 701) and Δq = 200 kPa (N = 1401)

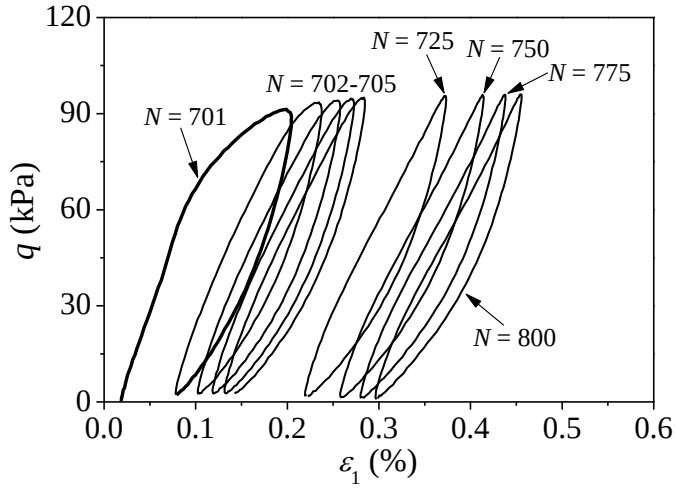

Fig. 12. Hysteresis loops during 100 cycles (N = 701 to 800) under Δq = 100 kPa for ballast sample at f_v = 20%

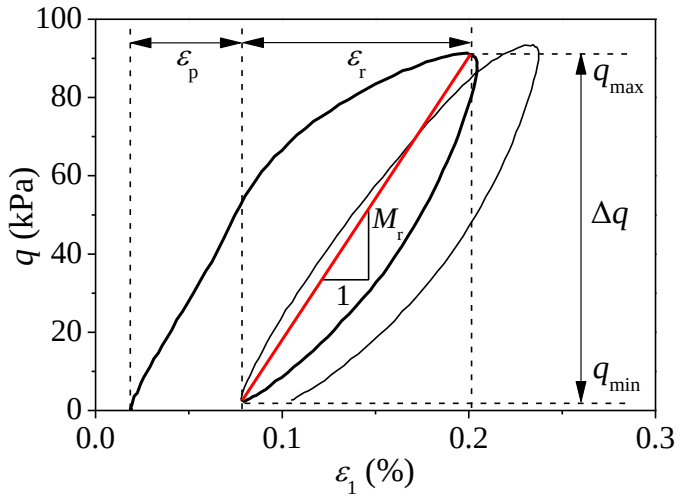

Fig. 13. Determination of M_r

Note: The two hysteresis loops shown are the testing results of ballast sample at f_v = 20% under Δq = 100 kPa at cycle numbers of N = 701 and 702.

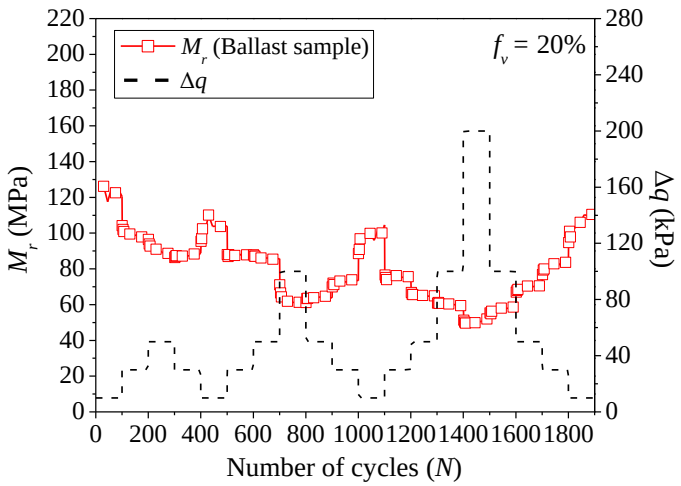

Fig. 14. Evolution of M_r with number of cycles at different stress levels for ballast sample at f_v = 20%

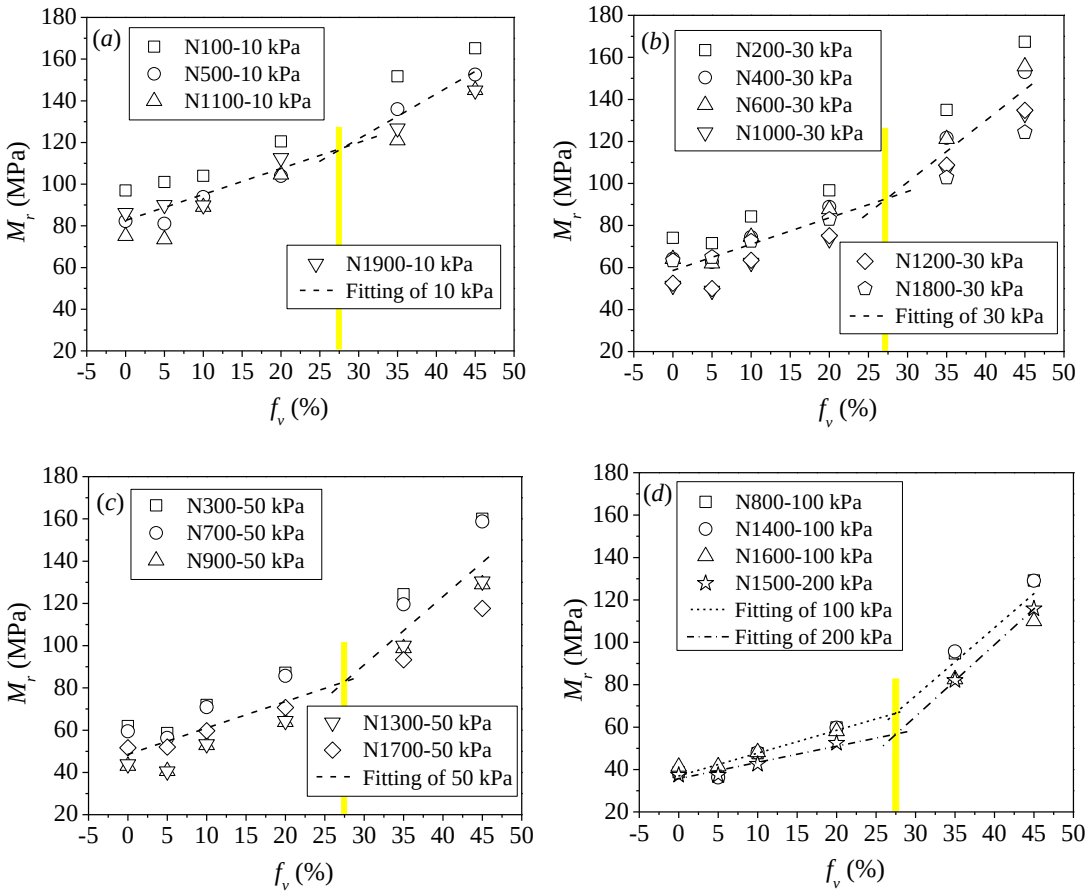

Fig. 15. Evolutions of M_r at end stage with f_v for ballast samples at: (a) Δq = 10 kPa; (b) Δq = 30 kPa; (c) Δq = 50 kPa; (d) Δq = 100 kPa and 200 kPa

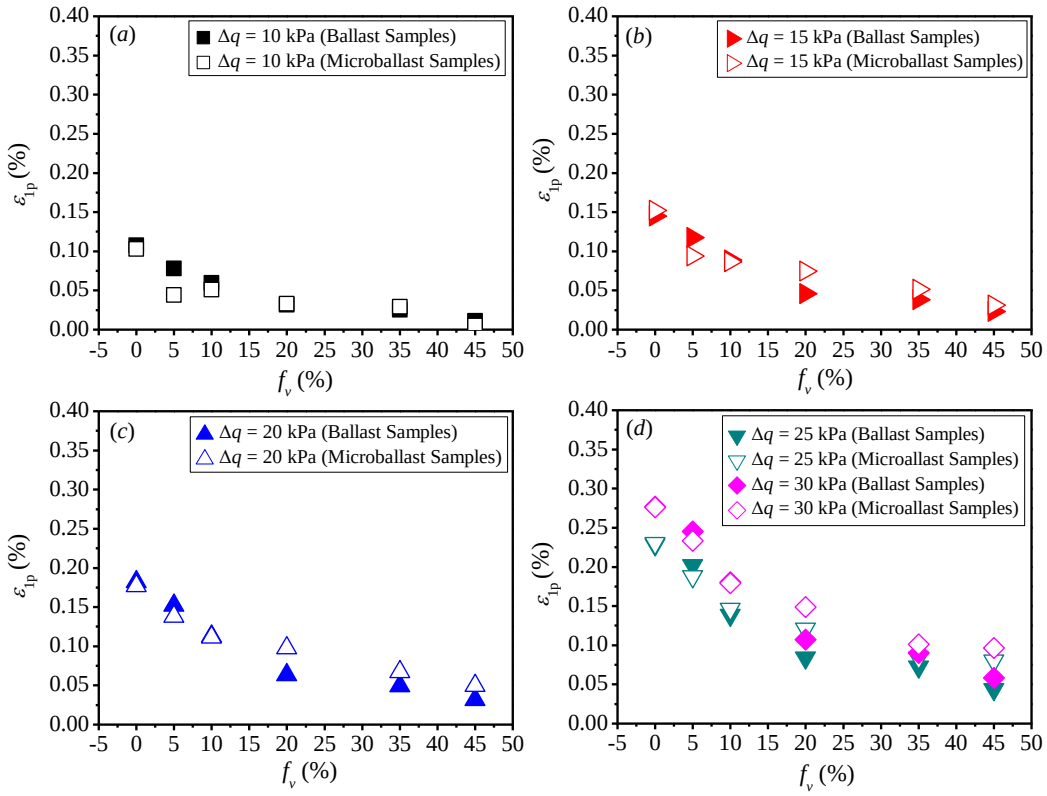

Fig. 16. Variations of estimated end-stage permanent strains with f_v for ballast and microballast samples at: (a) Δq = 10 kPa; (b) Δq = 15 kPa; (c) Δq = 20 kPa; (d) Δq = 25 kPa and 30 kPa

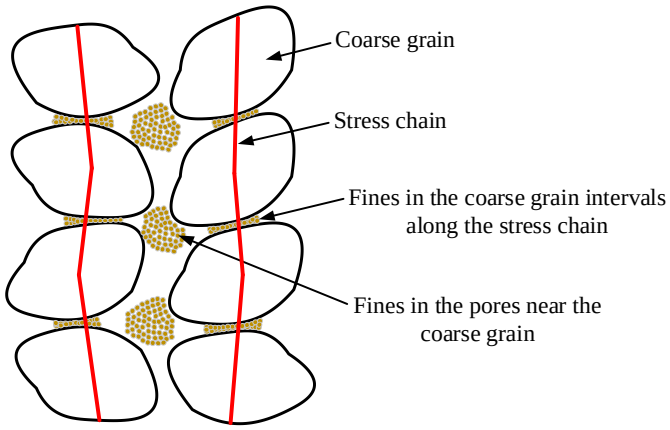

Fig. 17. Schematic illustration of the distribution of fines soils in case of grain-grain contact structure

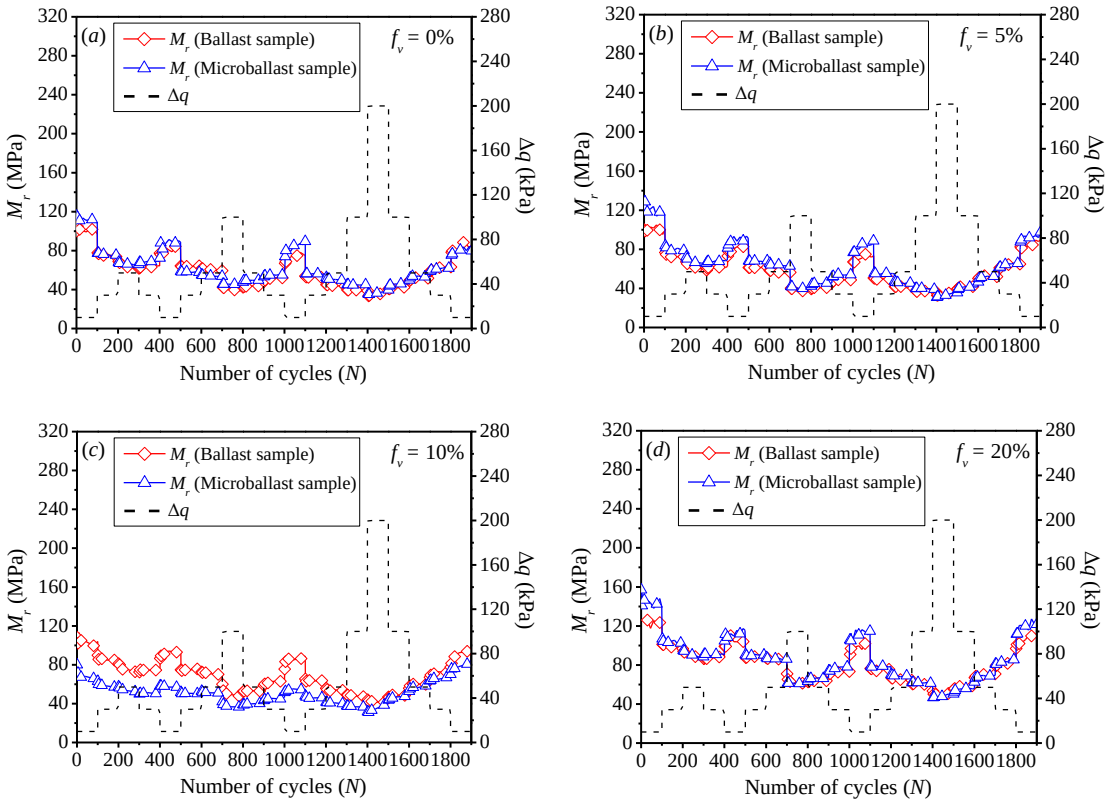

Fig. 18. Comparison of M_r value between ballast samples and microballast samples in case of fine-fine contact structure for: (a) f_v = 0%; (b) f_v = 5%; (c) f_v = 10%; (d) f_v = 20%

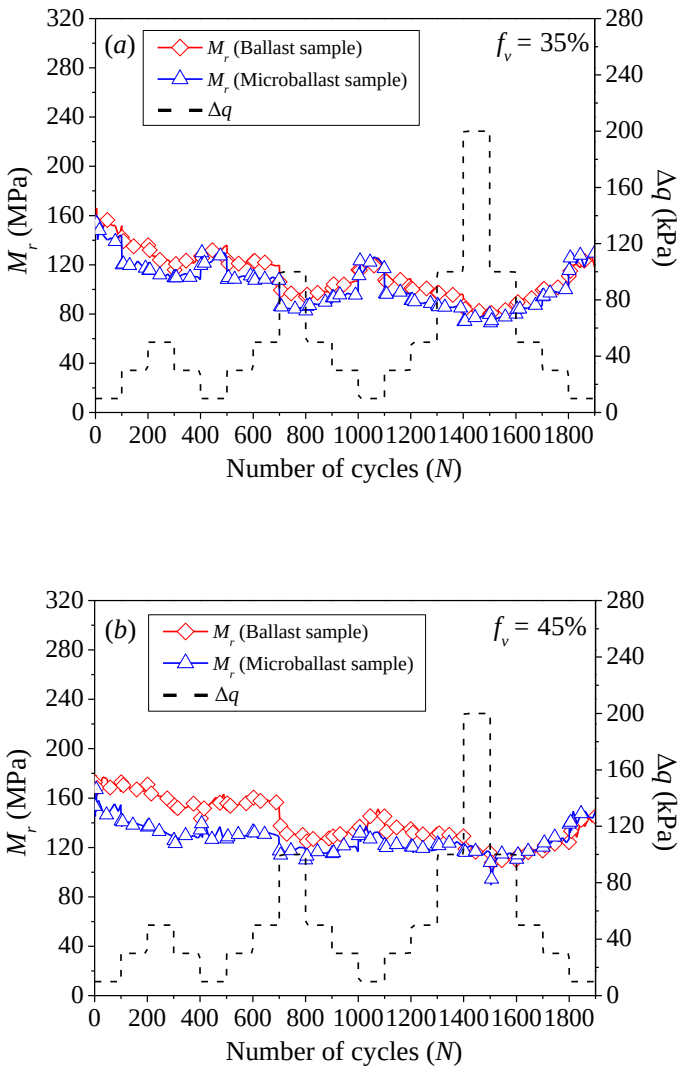

Fig. 19. Comparison of M_r value between ballast samples and microballast samples in case of grain-grain contact structure for (a) f_v = 35% and (b) f_v = 45%